General Disclaimer

One or more of the Following Statements may affect this Document

- This document has been reproduced from the best copy furnished by the organizational source. It is being released in the interest of making available as much information as possible.

- This document may contain data, which exceeds the sheet parameters. It was furnished in this condition by the organizational source and is the best copy available.

- This document may contain tone-on-tone or color graphs, charts and/or pictures, which have been reproduced in black and white.

- This document is paginated as submitted by the original source.

- Portions of this document are not fully legible due to the historical nature of some of the material. However, it is the best reproduction available from the original submission.

Produced by the NASA Center for Aerospace Information (CASI)

NASA TECHNICAL MEMORANDUM

NASA TM 78220

PROPELLANT GRAIN DYNAMICS IN AFT ATTACH RING OF SHUTTLE SOLID ROCKET BOOSTER

By V. Verderaime
Systems Dynamics Laboratory

(NASA-TM-78220) PROPELLANT GRAIN DYNAMICS IN AFT ATTACH RING OF SHUTTLE SOLID ROCKET BOOSTER (NASA) 47 p HC A03/MF A01 CSCL 21H

N79-20263

Unclas

G3/28 17277

February 1979

NASA

George C. Marshall Space Flight Center
Marshall Space Flight Center, Alabama

APR 1979
RECEIVED
NASA STI FACILITY
ACCESS DEPT.

MSFC - Form 3190 (Rev June 1971)

Page intentionally left blank

TABLE OF CONTENTS

LIST OF ILLUSTRATIONS

LIST OF TABLES

LIST OF TABLES (Concluded)

TECHNICAL MEMORANDUM 78220

PROPELLANT GRAIN DYNAMICS IN AFT ATTACH RING OF SHUTTLE SOLID ROCKET BOOSTER

I. SUMMARY

The dynamic modulus of solid propellant grains is known to depend significantly on temperature and frequency, but equally important is the dynamic strain amplitude in excess of 10^{-4}. This can be a troublesome property in dynamics analysis because the absolute amplitude of motion throughout the grain structure must be anticipated in order to select the real modulus from propellant test data.

A practical method is presented for determining the Solid Rocket Booster (SRB) grain modulus in the aft attach ring of Shuttle-mated vehicles during lift-off. It is essentially a plane unsymmetrical ring mode analysis using an existing structural dynamics program, but inherent procedures may be extended to other grain vibration problems.

The analytical method is demonstrated in the resolution of the flight vehicle dynamic modulus over a probable range of pitch excitations during lift-off.

II. INTRODUCTION

The unusual tangential mounting of the SRB onto the external tank (ET) at the aft attach ring was suspected of causing such large deformations of the grain cross section during pitch excitation that a critical selection of the propellant stiffness was required for the dynamic math model.

The purpose of this study was to specifically determine the dynamic real modulus existing in the SRB flight vehicles during lift-off. The analysis was limited to the cross section of the grain in the ring but inherent procedures would be extended to other grain structures if indicated.

The predominant effort was in developing practical techniques to determine the dynamic strain of the grain as a function of absolute modal amplitudes which had to be related to external excitation. Additional propellant tests were required to include frequencies from 1 to 5 Hz with a range at least an order of magnitude of dynamic strain variations and at different temperatures.

The Mated Vehicle Ground Vertical Test (MVGVT) data were used to determine the actual behavior of the SRB aft attach ring. The method for determining the dynamic strain and dynamic modulus was demonstrated using the excitation data at the ring and the fundamental frequency of the mated system. Ultimately, the MVGVT data and live propellant properties at extreme launch temperatures were projected to determine the grain modulus at the attach ring on flight vehicles during lift-off.

It is hoped that the liberal documentation of this study will provide useful insights for application to future propellant improvement programs.

III. FREE VIBRATION OF RING-GRAIN COMPOSITE STRUCTURE

The propellant grain outer diameter is bonded to the inner surface of the SRB aft attach ring. The ring is tangentially supported and accelerated as sketched in Figure 1. A free vibration analysis of this composite structure was conducted to identify and define relationships of all pertinent dynamic parameters affecting the grain stiffness before determining the dynamic modulus existing during forced excitation.

This analysis included a screening of environments affecting dynamic parameters, a development of absolute dynamic strain from modal analysis, and testing considerations for deriving supplementary propellant data. This part of the study progressed in that order and only a minimum of details are excluded.

A. Dominant Operational Environments

The operational environments that have the most effect on the propellant grain stiffness in the aft attach ring are those existing during lift-off; i.e., grain temperature, pitch acceleration, and combustion pressure.

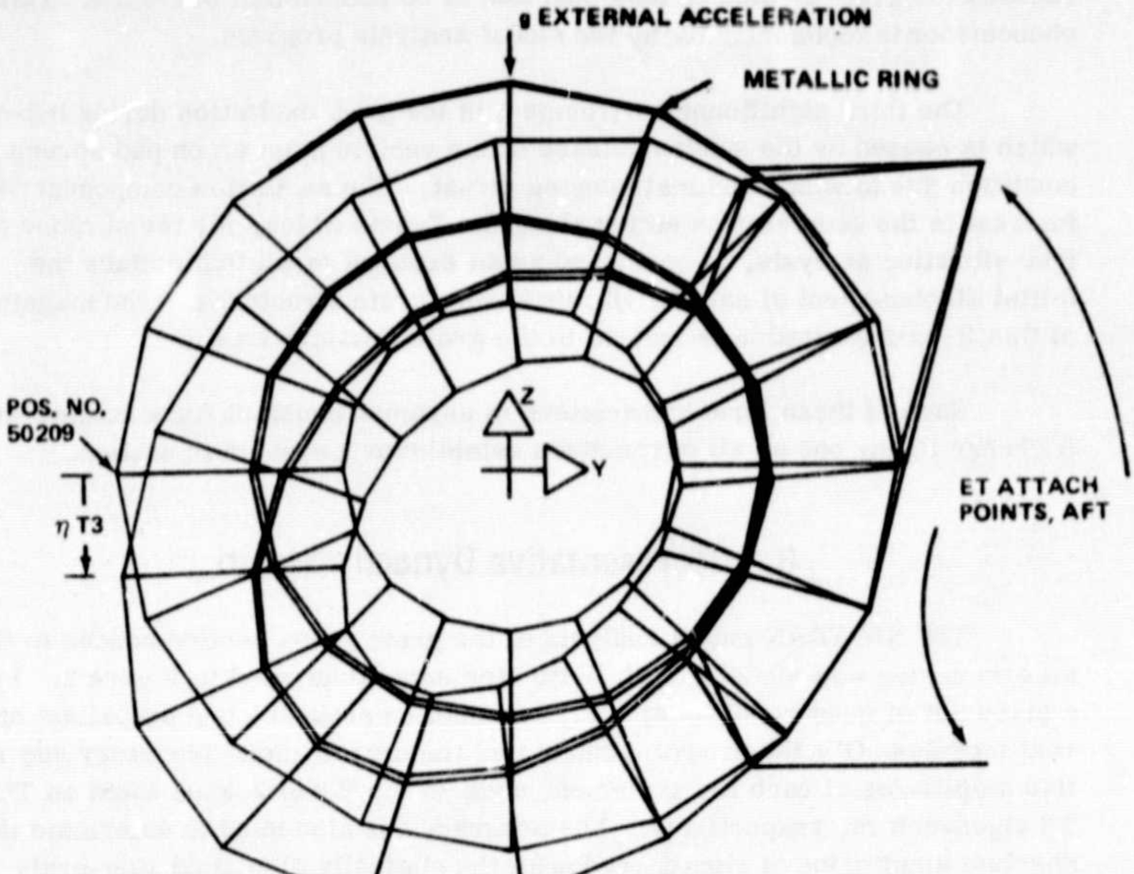

Figure 1. Grain cross section displacement due to Z-axis acceleration at SRB ring station 1511.

The propellant real modulus increases significantly over the anticipated ambient range of 90° to 40°F. For any given lift-off day, the grain temperature is reasonably uniform throughout the cross section so that only dynamic properties of the propellant at constant temperatures need to be considered.

The combustion pressure acting in the grain cavity imposes no direct grain strain. Propellant has a Poisson ratio of nearly 0.5 and is restrained by the relatively stiff metal ring so that no grain displacements can occur due to pressure. However, the incompressible grain will transmit the combustion pressure faithfully to the laterally vibrating ring which reduces the amplitude through nonlinear shell effects. This reduction of ring vibration amplitude reduces the grain strains to less than that of no combustion pressure. This phenomenon is accommodated by the modal analysis program.

The third significant environment is the pitch excitation during lift-off, which is caused by the sudden release of the vehicle from an on-pad sprung condition due to winds and main engine thrust. The excitation component of interest is the acceleration acting along the Z-axis which, for the purpose of free vibration analysis, is conceived as an external force that defines the initial displacement of natural vibrating ring-grain structures. The magnitude of this Z-axis excitation is related to the grain dynamic strain.

Each of these three parameters is assumed constant for a configuration. A change in any one or all parameters establishes a new configuration.

B. Representative Dynamic Strain

The NASTRAN modal analysis of the grain cross section bonded to the aft attach ring was modeled with finite elements illustrated in Figure 2. For a given set of input conditions, i.e., combustion pressure and propellant shear real modulus, G', the program calculated the natural mode frequency and relative amplitudes of each finite element node in the Y and Z axes noted as T2 and T3 eigenvectors, respectively. The program was also used to determine the absolute amplitudes of element nodes for the statically displaced ring-grain structure at one earth gravity acceleration. Both established the method for determining an absolute representative dynamic strain of the propellant grain.

1. Relative Strains from Modal Analysis. A typical finite element with notations and conversions used to define radial, tangential, and shear strains is presented in Figure 3. Notations and symbols used in Equations (1) through (8), though not conventional to structural analysis, were devised to conform to Tektronix computer programming. Because of the repetitive nature of applying these equations to each finite element and averaging, this program was developed and a printout is provided in the appendix.

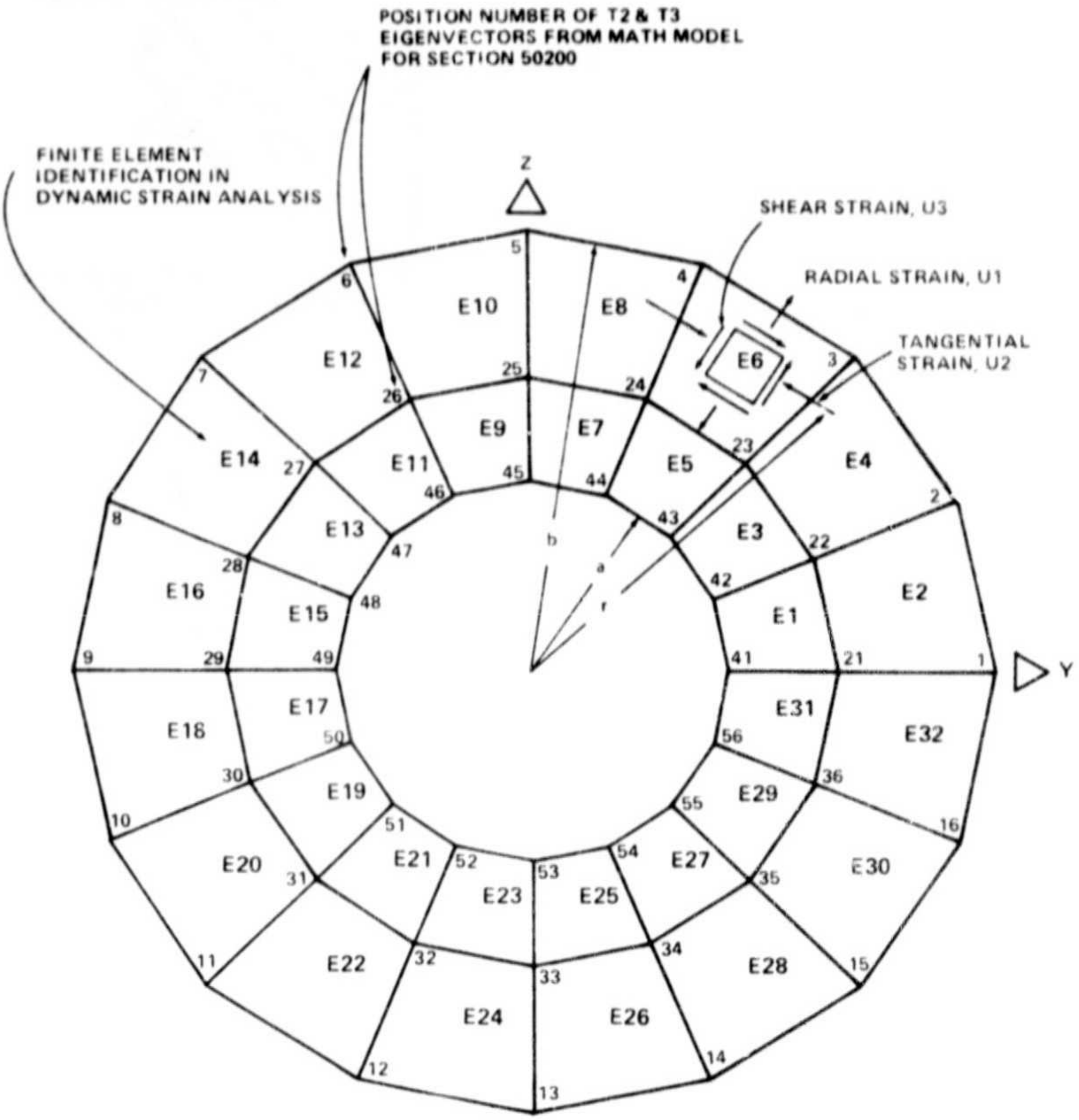

Figure 2. SRB grain cross section with finite element identification and typical strains.

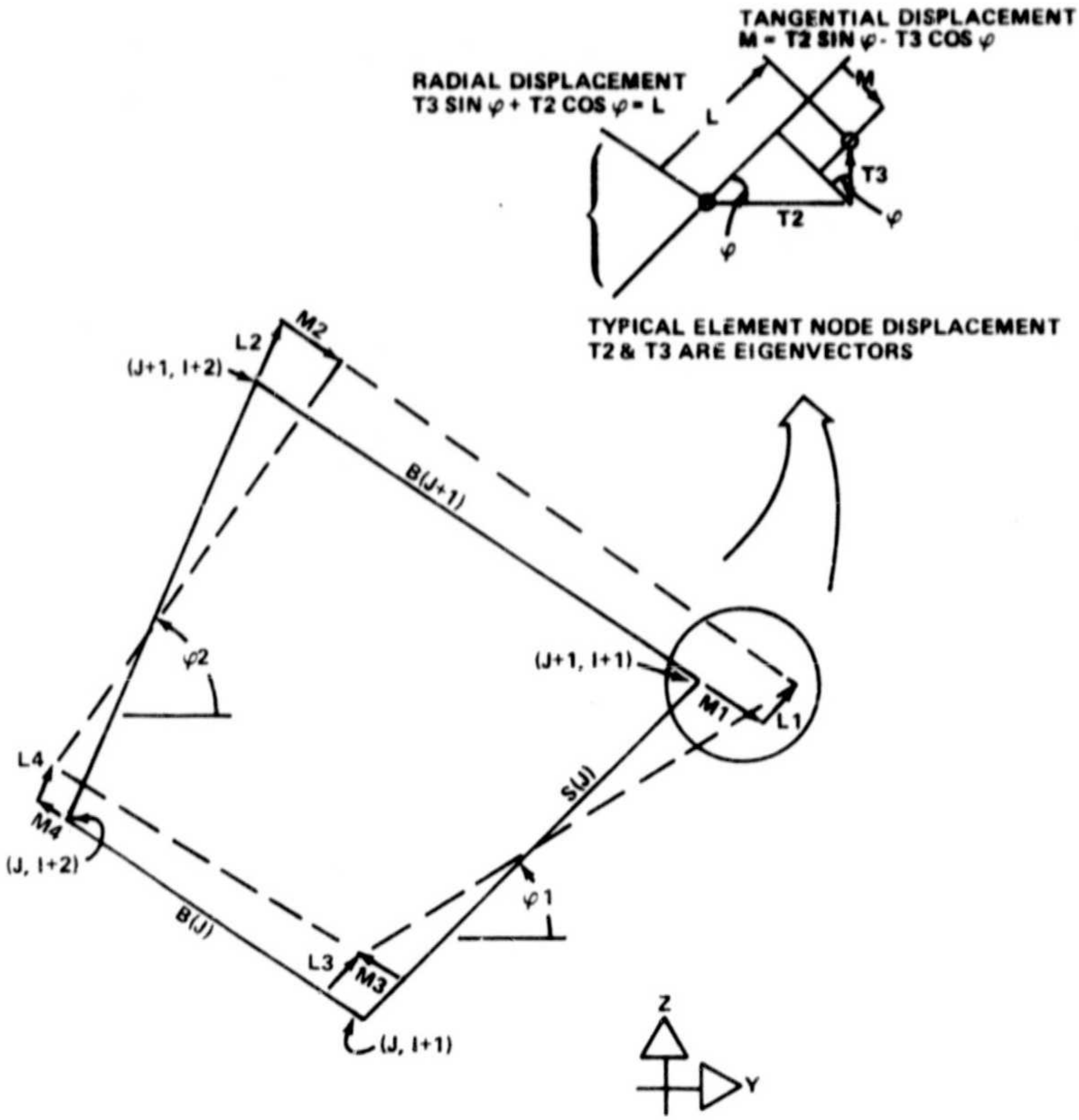

Figure 3. Finite element (typical) with coordinates and notations used in Equations (1) through (8).

Conversion of eigenvectors to relative radial and tangential displacements, L and M respectively, was obtained from

$$\left.\begin{aligned}
L1 &= T2(J+1,\ I+1)\ \cos\phi(1) + T3(J+1,\ I+1)\ \sin\phi(1)\\
L2 &= T2(J+1,\ I+2)\ \cos\phi(2) + T3(J+1,\ I+2)\ \sin\phi(2)\\
L3 &= T2(J,\ I+1)\ \cos\phi(1) + T3(J,\ I+1)\ \sin\phi(1)\\
L4 &= T2(J,\ I+2)\ \cos\phi(2) + T3(J,\ I+2)\ \sin\phi(2)
\end{aligned}\right\} \tag{1a}$$

$$\left.\begin{aligned}
M1 &= T2(J+1,\ I+1)\ \sin\phi(1) - T3(J+1,\ I+1)\ \cos\phi(1)\\
M2 &= T2(J+1,\ I+2)\ \sin\phi(2) - T3(J+1,\ I+2)\ \cos\phi(2)\\
M3 &= T2(J,\ I+1)\ \sin\phi(1) - T3(J,\ I+1)\ \cos\phi(1)\\
M4 &= T2(J,\ I+2)\ \sin\phi(2) - T3(J,\ I+2)\ \cos\phi(2)
\end{aligned}\right\} . \tag{1b}$$

The relative radial strain of each element was defined by

$$U1 = \frac{(L1 + L2 - L3 - L4)}{2S\,(J)} \quad ; \tag{2}$$

the relative tangential strain was defined by

$$U2 = \frac{(M1 - M2)}{2B(J+1)} + \frac{(M3 - M4)}{2B(J)} \quad ; \tag{3}$$

and the relative shear strain was defined by

$$U3 = \frac{(M1 + M2 - M3 - M4)}{2S(J)} + \frac{(L1 - L2)}{2B(J+1)} + \frac{(L3 - L4)}{2B(J)} \quad ; \tag{4}$$

where

$$A(J) = [R^2(J+1) - R^2(J)]\,\pi/N \tag{5}$$

is the element area and

$$\left.\begin{aligned} S(J) &= R(J+1) - R(J) \\ B(J) &= R(J)\ 2\pi/N \\ B(J+1) &= R(J+1)\ 2\pi/N \end{aligned}\right\} \tag{6}$$

are side lengths of the elements. The number of elements, N, dividing the cross section circle is 16.

The three relative strains of Equations (2), (3), and (4), acting simultaneously, were combined into a single familiar parameter (relative dynamic strain) through the strain energy density concept from elastic theory. The strain energy per unit volume may be expressed without stress terms by

$$W = 0.5\,\lambda e^2 + \left(\epsilon_r^2 + \epsilon_\theta^2\right) G + 0.5\,\gamma^2\, G' \quad ,$$

where G' is the shear modulus. The volumetric change, e, of a relatively incompressible propellant is zero which eliminates the first term of the equation. The shear strain, γ, can be reduced to zero by replacing the radial strain, ϵ_r, and tangential strain, ϵ_θ, with the maximum and minimum principal strains

$$F1,\ F3 = 0.5\,(U1 + U2) \pm 0.5\ [(U1 + U2)^2 + (U3)^2]^{0.5} \quad . \tag{7}$$

These are relative principal strains since relative strains of Equations (2), (3), and (4) are used.

Substituting these principal strains into the strain energy density equation and rearranging, the relative dynamic strain squared for each element is given by

$$(F4)^2 = (F1)^2 + (F3)^2 = W/G' \quad .$$

The relative dynamic strain of each finite element varies over the unsymmetrically displaced grain cross section. However, to reduce the computational complexity, grain properties are averaged over the grain total area. Accordingly, the average relative dynamic strain is

$$F4 = \left[\frac{\sum_{J=1}^{M} \sum_{I=1}^{N} [F1^2 + F2^2](I, J) A(I, J)}{N \sum_{J=1}^{N} A(J)} \right]^{1/2} \quad , \qquad (8)$$

resulting from modal analysis with a real shear modulus input of G'.

2. Absolute Amplitude of Dynamic Strain. If the absolute displacement of one finite element node point could be established, it would then follow that the dynamic strain absolute value would equal Equation (8) by a proportionality factor. A method for obtaining the real displacement of a finite element node was realized by using the same modal analysis program to obtain the absolute deflection of the supported ring-grain structure illustrated in Figure 1 with a 1-g static load acting along the Z-axis. This is a fair simulation of a known force imposed on the structure to produce an absolute initial displacement before releasing it to vibrate freely with that amplitude. It is also a good representation of the ring force excitation at the attach fitting by a known pitch acceleration g during lift-off.

The relationships of parameters between the static and modal system were derived from the normal mode equation of motion without damping

$$\ddot{\eta}_i + \omega_i^2 \eta_i = Q_i \quad ,$$

where η_i are the normal coordinates defined by the coordinate transformation

$$w(y, t) = \sum_{i=1}^{n} \phi_i(y) \eta_i(t)$$

in which $w(y, t)$ is the deflection of a point in the displacement configuration $\phi_i(y)$ of a vibrating system in the i^{th} natural mode. Applying an external force $F(y_j, t) = m(y_j, t)\, g$ and using deflections of the coordinate transformation equation, the virtual work is

$$\delta W = \sum_{j=1}^{m} F(y_j, t)\ \delta w(y_j, t) \quad ;$$

and in normal coordinates it is

$$\delta W = g \sum_{j=1}^{m} m(y_j) \left[\sum_{i=1}^{n} \phi_i(y_j)\ \delta\eta_i \right] \quad .$$

Rearranging and equating with the virtual work obtained from the generalized force

$$\delta W = \sum_{i=1}^{n} Q_i\ \delta\eta_i = g \sum_{i=1}^{n} \delta\eta_i \sum_{j=1}^{m} m(y_j)\ \phi_i(y_j) \quad ,$$

one obtains

$$Q_i = g \sum_{j=1}^{m} m(y_j)\ \phi_i(y_j) \quad .$$

Substituting this into the preceding equation of motion and letting $\ddot{\eta}_i = 0$ for static deflection and $\omega_i^2 = k_i$ for generalized mass normalized to unity, the normal coordinate for the deflected system is

$$\eta_i = \frac{g}{k_i} \sum_{j=1}^{m} \phi(y_j)\, m(y_j) \quad .$$

Identifying the static system by subscript "0" and the fundamental mode system by no subscript, one can establish the ratio between the normal coordinates of the two systems as

$$\eta = \eta_0 \left[\frac{g}{k}\right] \left[\frac{k_0}{g_0}\right] \quad .$$

The static absolute displacement ΔZ_0 of a finite element node point is related to the eigenvector T3 of the corresponding node of the fundamental mode system by

$$\Delta Z_0 = \eta_0 \, T3 \quad .$$

The node point used in this study is identified by position No. 50209 in the modal analysis printout. The stiffness, k, is the combined metal ring stiffness, C, in parallel with the propellant grain real modulus related by

$$k = (C + G') \quad .$$

Substituting both expressions into the preceding normal coordinates equation, one obtains

$$\eta = \frac{\Delta Z_0}{T_3} \left[\frac{C + G'_0}{g_0}\right] \left[\frac{g}{C + G'}\right] \quad , \tag{9}$$

which is the desired factor by which to multiply Equation (8) to convert relative strain to absolute dynamic strain

$$\epsilon_d = \eta(F4) \quad . \tag{10}$$

Since all propellant properties are determined from shear tests, the tensile dynamic strain, ϵ_d, is converted to shear dynamic strain, γ_d, by equating the tension strain energy density of $\eta(F4)$ in Equation (10) with the shear strain energy density of a lap shear specimen

$$W = \eta^2(F4)^2 G' = \gamma^2 G'/2 \quad .$$

The resulting conversion is

$$\gamma_d = \sqrt{2}\,\eta(F4) = \sqrt{2}\,\epsilon_d \quad .$$

Solving for η and substituting into equation (9), the dynamic shear strain of the free vibrating grain structure with initial condition g is

$$\gamma_d = gDP \quad . \tag{11}$$

Where the static parameters are lumped into the constant

$$D = \frac{\Delta Z_0}{g_0}\,(C + G'_0)\,\sqrt{2} \quad , \tag{12}$$

and g_0 is unity. The modal system parameters are expressed by

$$P = \frac{F4}{T3\,(C + G')} \quad . \tag{13}$$

The metal ring stiffness in Equations (12) and (13) is determined from two static deflection analyses. One uses only the ring with the propellant modulus equal to zero; the other uses some arbitrary value of G'_0 greater than 300 to obtain ΔZ_s and ΔZ_0 deflections, respectively, at the same finite element node point used in Equation (9). Equating the two results, the stiffness constant is calculated by

$$C = \frac{\Delta Z_0 \, G'_0}{\Delta Z_s - \Delta Z_0} \quad . \tag{14}$$

This constant must be calculated for each SRB ring configuration having a different stiffness due to changes in geometry or combustion pressure.

C. Digest of Stiffness Parameters

It is now appropriate to briefly recall sources and models already discussed by which the eight parameters identified act simultaneously to define the propellant grain stiffness. The modal analysis must satisfy the environment conditions and be compatible with propellant characteristics.

Three of these parameters originated from lift-off environments. The combustion pressure, p, is an input to the modal analysis which effectively stiffens the metal ring. It is also used in the static analysis to determine the ring parameter, C, by Equation (14). The pitch excitation, g, is assumed to initiate the free vibration absolute amplitude by which absolute dynamic strain, γ, is calculated in Equation (11). The ambient temperature, T, is used to estimate the grain temperature which grossly affects the propellant stiffness as determined from propellant dynamic test. Results from any grain modulus analysis at lift-off must address these three environment parameters.

The shear real modulus, G', is the desired value to define the propellant grain stiffness in this study. It is also the most significant propellant parameter input to the modal analysis from which the fundamental frequency, ω, is obtained as well as the eigenvectors by which the relative dynamic strain of Equation (8) is calculated. Another real modulus, G'_0, is used in the static analysis to determine the ring constant, C, of Equation (14).

Of these eight parameters, three are accounted for in the modal program and five are embodied in Equation (11) but temperature is not directly required by either one.

Finally, the restraining model of the four parameters already cited is provided by the propellant behavior determined from dynamic test data. These parameters are the real modulus, dynamic strain, frequency, and temperature (sometimes referred to as propellant properties). They are related by

$$G' = \frac{a \ \omega^{c}}{T^{b} \ \gamma_d^{e}} \quad , \tag{15}$$

where a, b, c, and e are determined by the test. However, these parameters are more conveniently plotted.

IV. PROPELLANT DYNAMIC PROPERTIES TEST

The primary purpose of the propellant test was to determine real moduli over a range of dynamic parameters anticipated for the MVGVT and the Orbiter Flight Test (OFT) vehicle service conditions. Pertinent test considerations were noted and resulting data were combined and smoothed to conform to specific trends.

A. Test Considerations

Because of the urgency for supplemental propellant data, general test requirements are based on relevant published information presented in References 1 through 5 and specific test consideration for facilities available follow.

1. Specimen Design. The lap shear type used by Rockwell International [2] appeared to best distribute applied test loads uniformly. It had the added advantage that its tester could accept a selection of large electrodynamic shakers to cover the desired range of dynamic strain amplitudes.

The specimen size had to be large enough to represent the properties of the bulk grain and had to repress effects of nontypical variations that might be manufactured into the grain by flow and settling patterns during casting and by localized temperature gradients during cure. The shear area could not exceed a 2- by 4-in. size because of the limited shaker force available for testing at the required low temperature and strain amplitude. The 1-in. thickness used by A. J. Yorgiadis [1] seemed to satisfy the instrumentation requirements and minimized the bonding material property effects over the propellant properties.

2. Static Strain Simulation. Usually test specimen are cut out of batch samples cured in flexible pasteboard cartons which preclude cure and thermal shrinkage strains. Consequently, their properties are somewhat different from propellants cured and stored in rigid motor casings.

As the cast propellant cures and drops to ambient temperature, T, the grain shrinks linearly by

$$H = [1 + 0.055\,(T - 145)] \times 10^{-3} \tag{16}$$

toward the bonded casing, and the inner radius increases and creates radial and circumferential strains

$$\epsilon_r = H(1 + \nu)\left[1 + \frac{b^2}{r^2}\right]$$

and

$$\epsilon_\theta = H(1 + \nu)\left[1 - \frac{b^2}{r^2}\right] \quad ,$$

respectively. The Poisson's ratio is taken as 0.5. Combining these strains and averaging over the grain cross section having an outer radius twice the inner radius results in a static strain of

$$\gamma_s \simeq 6H \quad . \tag{17}$$

It was recognized that this static strain develops over many hours which allows the stress and, therefore, the associated modulus to decay nearly as rapidly as it is applied. Also, the static strain then remains relatively constant through the SRB storage life with a static modulus less than half the initial value. The significance of the static strain is that, once incurred, the material structure may be permanently weakened to the extent that subsequently imposed strains will exhibit a lower modulus due to separation of filler-binder adhesion of the uniform mixture.

To simulate static strain on test specimens at a real time rate is unthinkable for the production type testing required. Instead, a parametric test was requested in which several levels of static strains were specified to be manually imposed and the modulus allowed to relax a minimum of 20 minutes prior to dynamic testing. If the modulus did not appreciably change at static strains up to 3 percent, this parameter would be ignored.

B. Test Data

Two distinct sources of data were used to compose the required dynamic properties of SRB propellant. Thiokol provided the statistical mean properties using one strain amplitude while RI provided supplemental data at lower frequencies and over a range of dynamic shear strains as shown in Table 1.

TABLE 1. PROPELLANT DATA SOURCE

	Thiokol	Rockwell International
Reference	2 and 6	7
Type Specimen	Gottenberg	Lap Shear
Number of Specimens per Temperature	18 or more	1 or 2
Frequency Range	5 to 50 Hz	1 to 20 Hz
Dynamic Strain Amplitude	0.008	0.001 to 0.014

1. Combining Data. Combining the two sources of data consisted of using the real modulus mean value at 5 Hz and 0.008 dynamic strain provided by Thiokol and superposing the 0.001 to 0.014 spread of dynamic strain provided by RI with both coinciding at the 0.008 strain curve as presented in Figure 4.

The real modulus obtained at 5 Hz from RI data was within the deviation range of Thiokol data except that the RI inert propellant was slightly higher. The real modulus deviation from specimen to specimen and batch to batch was approximately 10 to 20 percent with the higher temperature propellant demonstrating the larger deviation. In general, the inert and live properties were very similar.

The dynamic strain slopes of both sources of data were almost identical at 5 Hz. Spacing between dynamic strain increments was noted to be logarithmic as expected of rubberlike materials. This was also noted in Reference 1. Dynamic strains were plotted smooth to compensate for spurious data points of the limited number of RI specimen used, but patterns and specific trends observed were preserved.

2. Static Strain. The effect of static strains to simulate cure and thermal shrinkage was not incorporated in Figure 4 and is not recommended for future analysis until it can be supported by a detailed test program. The real modulus was expected to decrease with increasing static strain [5] but the reverse occurred. This could be indicative of unaccounted compression which increased the friction between the binder and filler, probably because of the specimen design and loading method. The preload application and relaxation rate needs to be developed for production type testing to reasonably simulate shrinkage conditions.

3. Data Results. The data provided satisfied all requirements except for static strain, which is a refinement generally ignored for probably the same difficulties encountered here. The composite development was better than expected because the two sources of data were reasonably compatible at the common superposition point of 5 Hz and 0.008 dynamic strain. Though dynamic strain properties only for 76° F ambient are presented for inert propellant, there are enough similarities between inert and live properties to admit sufficient extrapolation and trends to estimate properties at any temperature within the 40° and 90° F range.

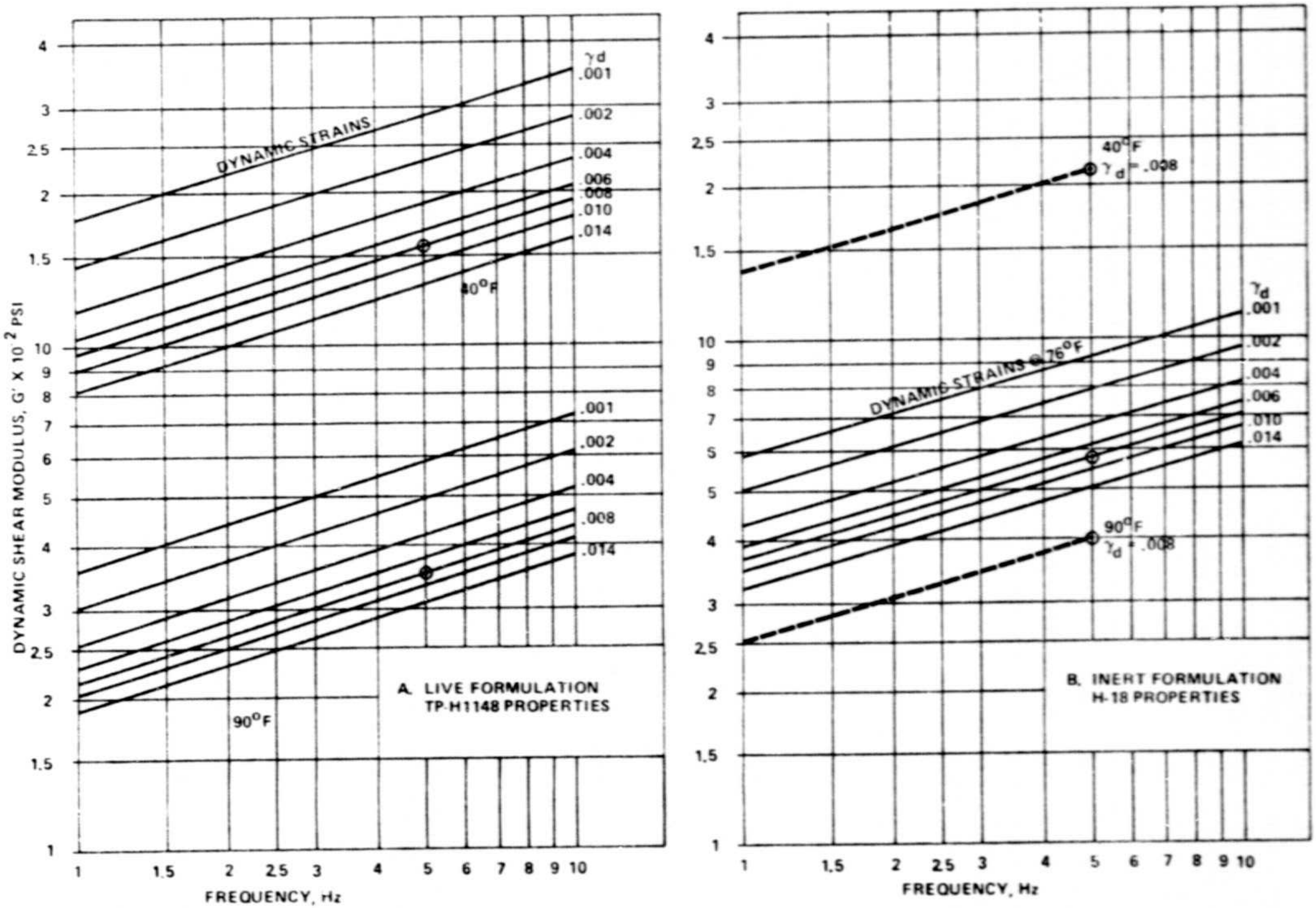

Figure 4. SRB propellant real modulus versus frequency and dynamic strains.

V. GRAIN MODULUS DETERMINATION

Having identified and interrelated the parameters influencing the grain dynamic real modulus, their utilization and procedure for determining the modulus is now demonstrated in application to MVGVT and OFT vehicles. The analysis is limited to the aft attach ring behavior and is consistent with the study scope. The MVGVT is treated first because of the required test data to define the actual dynamic behavior of the Shuttle mated system and resulting environment on the SRB at the ring station 1517. The lift-off response was then assumed to be dominated by the MVGVT system fundamental mode.

A. MVGVT Vehicle

In tracking those parameters directly affected by test environments, two MVGVT configurations were noted: a 0-psi and a 600-psi combustion pressure simulation. Because the two configurations were tested a month apart, temperature parameters were expected to be significantly different.

It was also noted that two fundamental modes were excited. The symmetrical mode consisted of the SRB elements vibrating with opposite angular accelerations at the aft attach ring level. The nonsymmetrical mode had both SRB vibrating with similar angular acceleration. Therefore, the pitch excitation parameter, g_M, of the two modes were different.

Figure 5 summarizes relevant MVGVT test data from which environment parameters of grain temperature and pitch excitation may be determined.

Configuration 1, with no combustion pressure simulation, was tested on October 26 and 31. For three consecutive days prior to the test, the average temperature was 65°F which was also believed to be that of the propellant grain. The second configuration, with a 600-psi pressure simulation, was tested on December 1 and 2 with a probable grain temperature of 50°F which was also based on a 3-day average ambient. Propellant properties at 50° and 65°F were constructed and are presented in Figure 6.

The average pitch excitation parameter, g_M, acting on the SRB ring along the Z-axis is bound by the acceleration diagram shown in Figure 5 and is calculated by

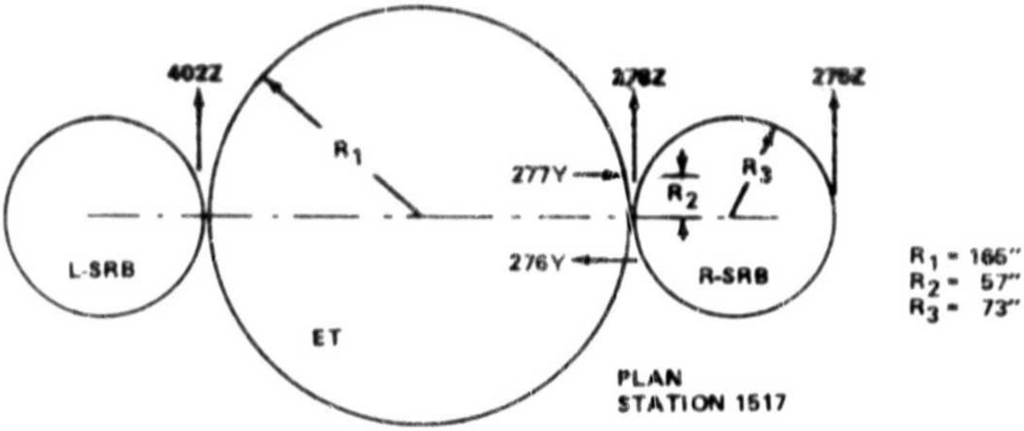

SIMULATED PRESSURE	MODE	TEST DATE	SYMME-TRICAL	SYSTEM ω_M, Hz
0	5	10-31-78	YES	2.0588
0	8	10-26	NO	2.2353
600 PSI	47	12-1	YES	2.0392
600 PSI	48	12-2	NO	2.2157

MODE	ACCELEROMETER DATA, g's				
	402Z	278Z	276Z	277Y	276Y
5	.0306	.0310	-.0279	.0166	-.0141
8	-.0146	.0142	-.0040	.0114	.0032
47	.0423	.0416	-.0447	.0223	-.0184
48	-.0387	.0372	-.0132	.0316	.0081

MVGVT TEST DATA

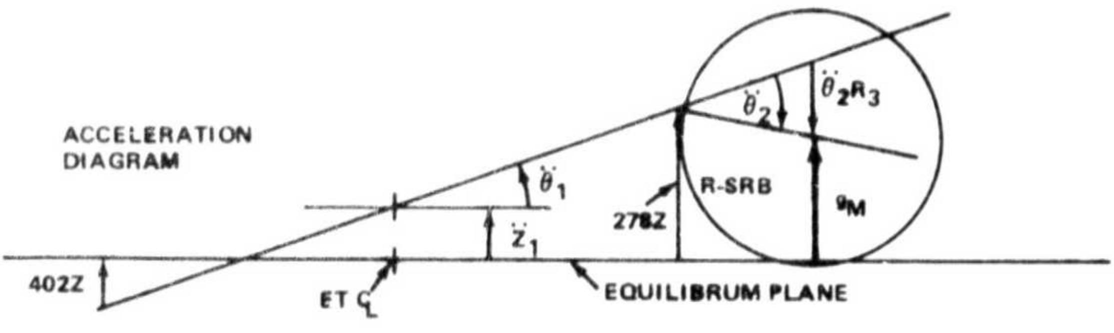

Figure 5. MVGVT test data and acceleration diagram.

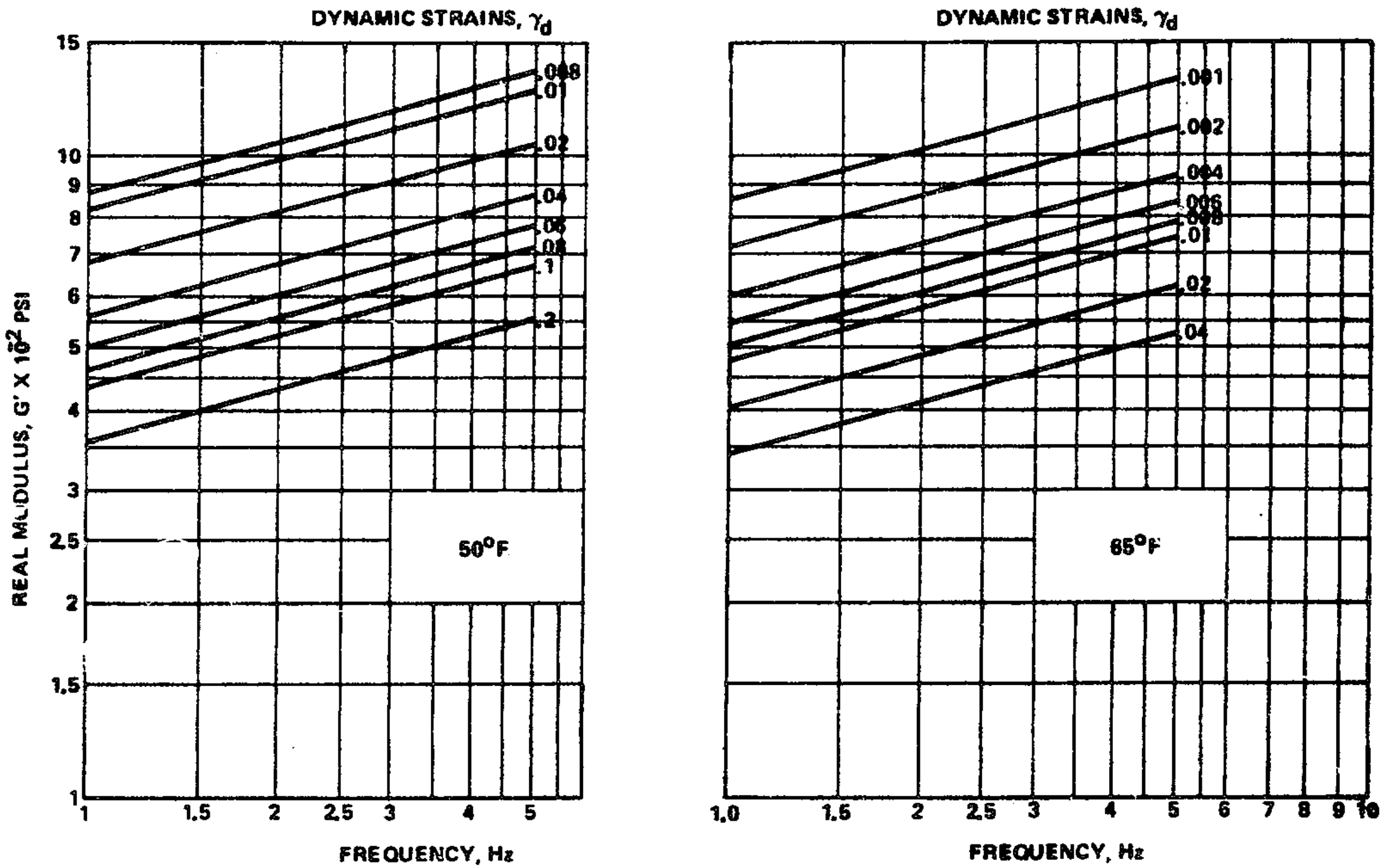

Figure 6. H-18 propellant properties extrapolated to MVGVT grain temperature.

$$g_M = \ddot{Z}_1 + \ddot{\theta}_1 R_1 \left(\frac{R_1 + R_2}{R_1}\right) - \ddot{\theta}_2 R_2 \left(\frac{R_3}{R_2}\right) \quad , \tag{18}$$

where

$$\left.\begin{aligned} \ddot{Z}_1 &= 0.5\,(278Z + 402Z) \\ \ddot{\theta}_1 R_1 &= 0.5\,(278Z - 402Z) \\ \ddot{\theta}_2 R_2 &= 0.5\,(277Y + 276Y) \end{aligned}\right\} \tag{19}$$

and the alphanumerics in parentheses are acceleration data of designated accelerometers (Figure 5).

Results of parameters from MVGVT test data are summarized in Table 2 where ω_M is the mated system fundamental frequency. This frequency is plotted as a function of pitch excitation, g_M, in Figure 7. Subscripts M refer to mated vehicle conditions.

TABLE 2. MVGVT ENVIRONMENTAL PARAMETERS

Configuration	Simulated Pressure (psi)	Grain Temperature (°F)	Test Mode	Symmetrical	System ω_M (Hz)	SRB Excitation g_M
1	0	65	5	Yes	2.059	0.030
			8	No	2.235	0.011
2	600	50	47	Yes	2.039	0.039
			48	No	2.215	0.030

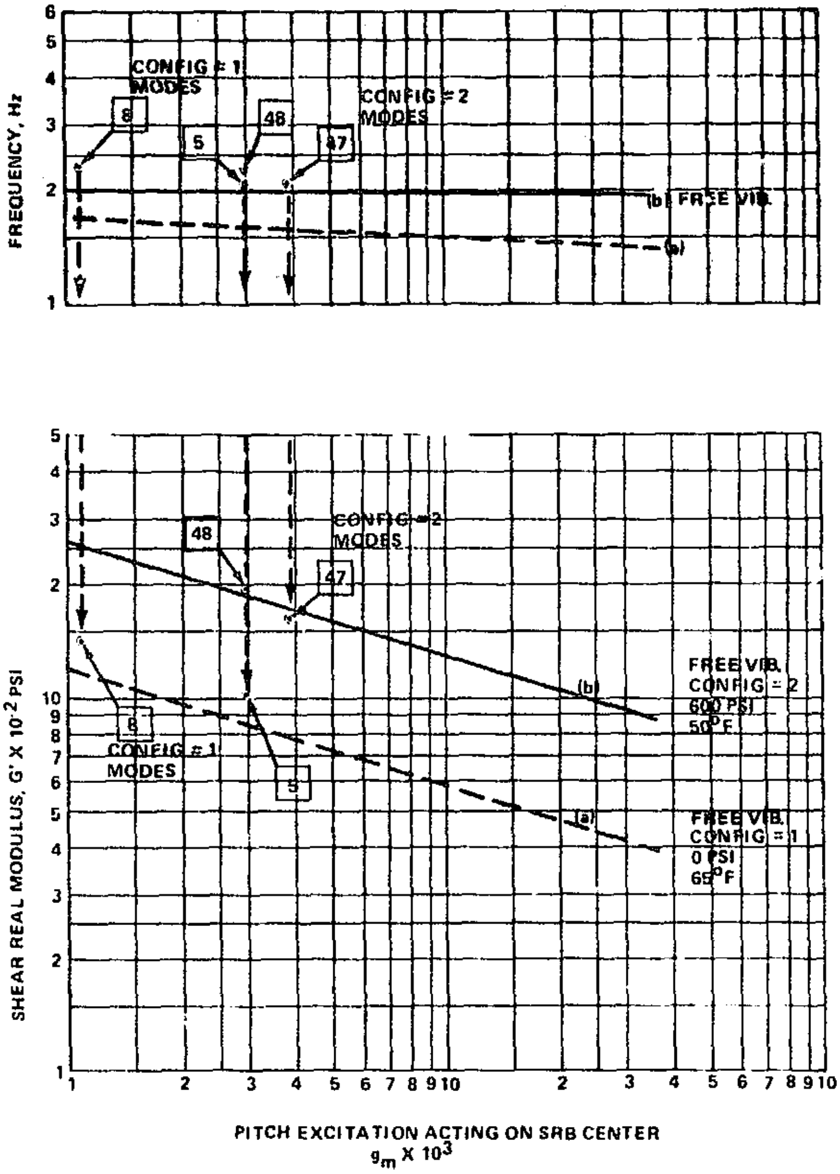

Figure 7. MVGVT propellant grain modulus.

The next step was to determine the frequency and modulus, G', of a free vibrating ring-grain structure if excited by the acceleration experienced in the MVGVT of Table 2. Using the modal analysis program, two arbitrary moduli were selected to establish curves (a) and (b) of Figure 7 which extends through the g_M excitations of MVGVT. Table 3 presents output data required to calculate P of Equation (13) as required by Equation (11). Table 4 presents the output data from the static analysis used to determine the metallic ring stiffness, C, of Equation (14) and the static constant, D, of Equation (12). Both are also required by Equation (11). The dynamic strain was selected

TABLE 3. MODAL OUTPUT

Simulated Pressure (psi)	G Assumed	ω (Hz)	T3 (209)	F4 (Eq. 8)	P (Eq. 13)
0	415	1.40	0.960	0.01149	1.915×10^{-5}
	800	1.58	0.962	0.01139	1.172×10^{-5}
600	415	1.87	0.901	0.01033	2.951×10^{-6}
	800	1.92	0.878	0.01008	2.688×10^{-6}

TABLE 4. STATIC SYSTEM DATA

Input		Output Deflection (in.)	C (Eq. 14)	D (Eq. 12)
Simulated Pressure (psi)	G Assumed			
0	$G_s = 0$	$\Delta Z_s = 16.58$	210	4920
	$G_0 = 400$	$\Delta Z_0 = 5.71$		
600	$G_s = 0$	$\Delta Z_s = 2.82$	3470	13,830
	$G_0 = 800$	$\Delta Z_0 = 2.29$		

from the MVGVT propellant data of Figure 6 for each set of modulus and natural frequency presented in Table 3 at appropriate temperatures obtained from Table 2. These properties are summarized in Table 5, which includes the excitation calculated by Equation (11) to induce the associated dynamic strains.

TABLE 5. MVGVT FREE VIBRATION SYSTEM

Configuration	Temperature (°F)	G'	ω	γ_d (Eq. 6)	g (Eq. 11)	Curve
1	65	415	1.40	0.025	0.265	a
		800	1.58	0.002	0.035	
2	50	415	1.87	0.20	4.90	b
		800	1.92	0.02	0.538	

The data presented in Table 5 are all that are necessary to establish curves (a) and (b) for moduli and frequencies over a range of excitations, g, plotted in Figure 7. It is also of interest to note that all parameters of any free vibrating system with a known initial excitation g cannot be derived by working backward through the established equations presented in paragraph III. B. (2) and the propellant properties of Figure 6 without the aid of curve (a) or (b).

The ring-grain structure in the MVGVT vibrates with the vehicle system fundamental frequency, which may not be the same as the free vibrating system though selected with the same excitation as in Figure 7. Therefore, the moduli are not the same. To determine the grain modulus acting during MVGVT, the relationship of motion between the two systems is investigated. The subscript M will refer to the forced system in the mated vehicle as before and n will refer to the free vibrating system.

The displacement of the free system with initial conditions set by g_M is calculated from Equation (9) as

$$Z_n = \eta T3 = \frac{\Delta Z_0}{g_0} (C + G_0') \frac{g_M}{(C + G_n')}$$

or

$$Z_n = g_M \frac{D}{\sqrt{2}\,(C + G_n')} \quad .$$

The displacement and acceleration relationship of the forced harmonic system is obtained in the usual way of differentiating displacement twice so that

$$Z_M = \frac{\ddot{Z}}{\omega_M^2} = \frac{g_M}{\omega_M^2} \frac{(32.2 \times 12)}{(2\pi)^2} \quad .$$

Solving for g_M in the displacement equation of both systems and equating, the ratio of the two systems is obtained as

$$r = \frac{Z_M}{Z_n} = \frac{(C + G_n')}{D\omega_M^2} \frac{(\sqrt{2} \times 32.2 \times 12)}{(2\pi)^2} \quad . \tag{20}$$

From curves (a) and (b), the free vibration system modulus and frequency is obtained for the g_M. Using these two properties in Figure 6, the dynamic strain is obtained. Since the dynamic strain of the propellant grain is proportional to displacement, the dynamic strain of the forced system is calculated by

$$\gamma_M = r\,\gamma_n \quad . \tag{21}$$

Using this dynamic strain, γ_M, and the frequency of the MVGVT system, ω_M, in Figure 6, the desired modulus G_M is resolved. Data of the two systems used to resolve the MVGVT modulus for each mode are presented in Table 6 and moduli, G_M, are plotted in Figure 7.

TABLE 6. MVGVT PROPELLANT GRAIN DATA

g_M	Mode	ω_n	G'_n	γ_n	ω_M	r	γ_M	G'_M
0.030	5	1.6	850	0.0017	2.039	0.70	0.0012	1000
0.011	8	1.7	1200	0.0004	2.235	0.79	0.0003	1400
0.039	47	2.0	1700	0.0015	2.039	1.24	0.0018	1600
0.030	48	2.0	1800	0.001	2.235	1.07	0.0011	1900

B. OFT Vehicles

Unlike the MVGVT, the OFT flight environments at lift-off are defined by broad ranges, but combustion pressure of the SRB may be assumed to be 600 psi at maximum excitation so that only one configuration will be analyzed. The extreme ambient temperatures specified are 40° and 90°F. Two fundamental modes for the mated vehicle system that influenced the pitch excitation parameter, g_M, were noted to exist: symmetrical and nonsymmetrical. Both modes will be considered for the OFT flight environment. Because ground winds and engine thrust at lift-off are variable contributors to pitch excitation of the mated vehicle, a range over one order of magnitude of acceleration will be investigated. Consequently, the OFT grain modulus in the aft attach ring will be resolved parametrically.

The pitch excitation parameter of Equation (18) may be more meaningfully defined for flight vehicles by referring it to the anticipated Z-acceleration at the attach fitting which corresponds to the accelerometer number 278Z location on the MVGVT. It is an interface point common to the Shuttle elements and design loads community. Then, OFT pitch acceleration acting on the SRB center is

$$\bar{g}_M = B\, g_F \quad , \tag{22}$$

where g_F is the anticipated acceleration at the fitting. Substituting MVGVT values for the symmetrical and nonsymmetrical modes, one obtains

$$\left.\begin{aligned} B_1 &= \frac{g_M}{g_{278Z}} = \frac{0.039}{0.041} = 0.95 \\ B_2 &= \frac{g_M}{g_{278Z}} = \frac{0.030}{0.037} = 0.81 \end{aligned}\right\} , \qquad (23)$$

respectively.

Table 7 summarizes the lift-off environment and parameters to be applied to the OFT modulus determination that covers extreme yearly operational conditions.

TABLE 7. OFT ENVIRONMENT PARAMETERS

Mode	Grain Temperature (°F)	System ω_M	B (Eq. 22)	g_F
Symmetrical	40	2.039	0.95	0.1 to 1.0
	90	2.039	0.95	0.1 to 1.0
Nonsymmetrical	40	2.215	0.81	0.1 to 1.0
	90	2.215	0.81	0.1 to 1.0

To establish curves (a) and (b) in Figure 8 of a free vibrating ring-grain structure as was done on MVGVT, Tables 3 and 4 were applicable again. Figure 4 was used to select the live propellant properties of γ_d listed in Table 8. The excitation, g, was calculated from Equation (11). Curves (a) and (b) of moduli and frequencies were extended through the excitation, g, range of 0.1 to 1.0 in Figure 8.

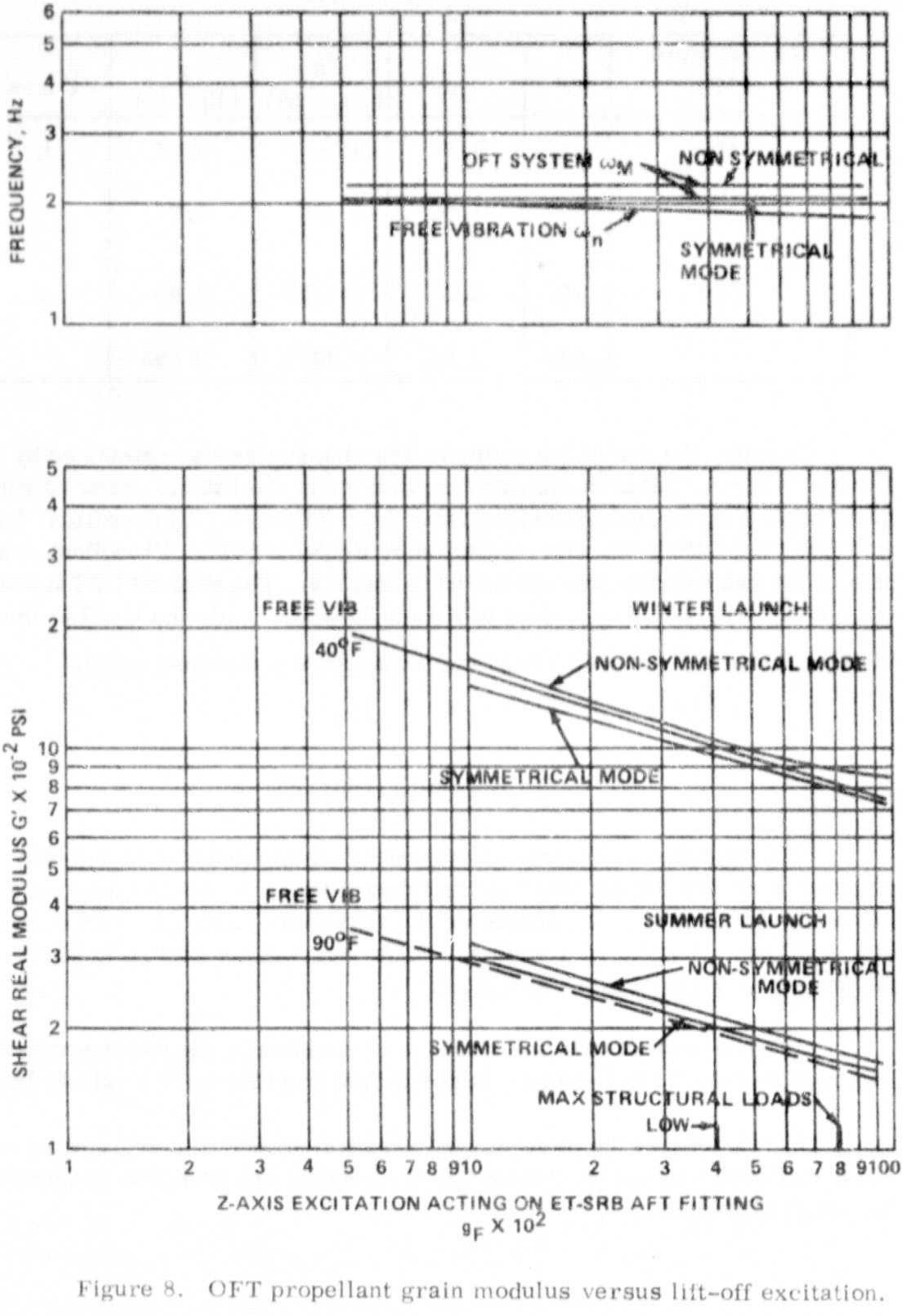

Figure 8. OFT propellant grain modulus versus lift-off excitation.

TABLE 8. OFT FREE VIBRATION SYSTEM

Temperature (°F)	G'	ω	γ_d (Fig. 4A)	g (Eq. 11)	Curve
40	415	1.87	0.28	6.86	b
	800	1.92	0.028	0.75	
90	415	1.87	0.0012	0.03	a
	800	1.92	0.00012	0.003	

Finally, the excitation acting on the ring center was calculated by Equation (22) for select anticipated excitations at the fitting. Free vibration moduli and frequencies were interpreted from Figure 8. The modified dynamic strain for the OFT grain was calculated by Equation (21). Propellant grain data of the two systems are presented in Table 9. The desired OFT moduli, G'_M, at 40° and 90°F are plotted in Figure 8, which is almost equal to that of the free vibrating system because the frequencies are almost equal.

VI. CONCLUSIONS

The objective to determine the grain dynamic modulus in the SRB aft attach ring during lift-off was accomplished through the development of a comprehensive analysis which considered the variation of dynamic strain property of propellant. Results of a study for flight vehicles are plotted in Figure 8, and pertinent observations were as follows:

1) The most significant variation of modulus is due to temperature. The real modulus increases by a factor of five from summer to winter launch.

2) Increasing the pitch excitation at lift-off due to increasing ground winds and engine thrust decreases the real modulus by less than 60 percent in the range of interest.

TABLE 9. OFT PROPELLANT GRAIN DATA

g_F	B	$\bar{g}_M$	Temperature (°F)	ω_n	G'_n	γ_n	ω_M	r	γ_M	G'_M
0.1	0.95	0.095	40	2.0	1550	0.0032	2.039	1.2	0.0038	1450
			90		300	0.0045		0.91	0.0040	300
	0.81	0.081	40		1650	0.0029	2.215	1.04	0.0030	1650
			90		310	0.0048		0.77	0.0037	330
0.3	0.95	0.285	40	1.95	1100	0.01	2.039	1.10	0.011	1050
			90		210	0.02		0.88	0.018	210
	0.81	0.243	40		1150	0.01	2.215	0.94	0.0094	1150
			90		220	0.019		0.75	0.014	240
1.0	0.95	0.95	40	1.90	750	0.034	2.039	1.01	0.0345	750
			90		150	0.075		0.87	0.065	160
	0.81	0.81	40		800	0.032	2.215	0.87	0.028	850
			90		160	0.070		0.74	0.052	170

3) The highest pitch excitations at the fitting anticipated for any launch day is 0.8 g_M and the lowest with negligible ground winds is 0.4 g_M. Design modulus for any day launch should range from 170 to 1000 psi.

4) SRB combustion pressure of 600 psi was used which indirectly doubled the grain modulus. Pressure buildup of less than 600 psi during lift-off will decrease the structure stiffness.

5) Grain dynamic strains resulting in the aft attach ring range from 0.01 to 0.07 for flight vehicles. Dynamic strains forward of the ring are much less. Dynamic properties data from propellant contractors should include a broad range of dynamic strain tests rather than the present practice of a single amplitude provided by References 2 and 6.

6) Simulation of SRB cure and storage static strains on test specimen should be formulated for production type testing.

APPENDIX

DYNAMIC STRAIN COMPUTER PROGRAM FOR SRB GRAIN CROSS SECTION

The strain analysis was programmed in Basic Language for the 4051 TEKTRONIX computer. Symbols used are the same as defined in paragraph III. B. (1) of this report with the exception of: (1) Y and Z replace the T2 and T3 eigenvectors used in Equation (1); (2) K is an optional conversion factor with no present assignment; and (3) P(I) and P(I+1) replace angles $\phi(1)$ and $\phi(2)$ of Equation (1) and Figure (3).

```
FIND 1
OLD
LIST
100 REMARK Propellant Grain Dynamic Strain Program
101 DELETE Y,Z,A,B,R,S
102 SET DEGREES
103 VIEWPORT 20,110,0,90
104 DIM Y(3,17),Z(3,17),A(2),B(3),R(3),S(2)
105 DATA 1,0.495,16,2,30.917,48,72.74
106 READ K,V,N,M,R
107 FOR J=1 TO M
108 S(J)=R(J+1)-R(J)
109 A(J)=PI*(R(J+1)↑2-R(J)↑2)/N
110 B(J)=2*PI*R(J)/N
111 NEXT J
112 B(M+1)=2*PI*R(M+1)/N
113 PRINT "L                                   Program Menu___ 1. Input Run ";
114 PRINT "ID                                                                _";
115 PRINT "2. Input number of sectors                Default = 16_ 3. Inp";
116 PRINT "ut number of annular rings          Default = 2_ 4. Input disp";
117 PRINT "lacement scale                  Default = 1_ 5. Input Poisson's r";
118 PRINT "atio                  Default = .495_ 6. Input annular ring ra";
119 PRINT "dii              Default = 30.917, 48, 72.74_ 7. Input displa";
120 PRINT "cements from tape file                 _ 8. Input displacements";
121 PRINT " from keyboard_ 9. Output displacements to tape file_10. Ou";
122 PRINT "tput element nomenclature_11. Output calculated element geo";
123 PRINT "metry_12. Output propellant dynamic strains  _13. Exit prog";
124 PRINT "ram__        Input line number of desired program response : ";
125 INPUT R1
126 GO TO R1 OF 129,132,137,165,168,154,229,212,238,142,194,244,127
127 PAGE           T$   N   M   K   V   R   ΔTape  ΔKey  To tape  Nom  geo  ...  Stop
128 END
129 PRINT "__Run ID = ";
130 INPUT T$
131 GO TO 113
```

ORIGINAL PAGE IS
OF POOR QUALITY

```
132 PRINT "__Number of sectors = ";
133 INPUT N
134 DELETE Y,Z
135 DIM Y(M+1,N+1),Z(M+1,N+1)
136 GO TO 107
137 PRINT "__Number of annular rings = ";
138 INPUT M
139 DELETE Y,Z,A,B,R,S
140 DIM Y(M+1,N+1),Z(M+1,N+1),A(M),B(M+1),R(M+1),S(M)
141 GO TO 154
142 PRINT "LRun ID = ";T$;"__Element Nomenclature"
143 WINDOW -R(M+1),R(M+1),-R(M+1),R(M+1)
144 FOR I=0 TO N-1
145 GOSUB 171
146 NEXT I
147 PRINT @32,21:115,45
148 PRINT @32,20:112,47,112,43,115,45
149 PRINT " Y"
150 PRINT @32,21:65,95
151 PRINT @32,20:63,92,67,92,65,95
152 PRINT "KZ"
153 GO TO 209
154 FOR I=1 TO M+1
155 IF I>1 THEN 158
156 PRINT "__Inner radius= ";
157 GO TO 162
158 IF I=M+1 THEN 161
159 PRINT "Intermediate radius= ";
160 GO TO 162
161 PRINT "Outer radius= ";
162 INPUT R(I)
163 NEXT I
164 GO TO 107
165 PRINT "__Displacement Scale, K= ";
166 INPUT K
```

ORIGINAL PAGE IS
OF POOR QUALITY

```
167 GO TO 113
168 PRINT "__Input Poisson's ratio, V= ";
169 INPUT V
170 GO TO 113
171 REMARK Sector Plotting Subroutine
172 P1=360*I/N
173 P2=P1+360/N
174 MOVE R(1)*COS(P1),R(1)*SIN(P1)
175 DRAW R(M+1)*COS(P1),R(M+1)*SIN(P1)
176 MOVE R(1)*COS(P2),R(1)*SIN(P2)
177 DRAW R(M+1)*COS(P2),R(M+1)*SIN(P2)
178 FOR J=1 TO M
179 MOVE R(J)*COS(P1),R(J)*SIN(P1)
180 DRAW R(J)*COS(P2),R(J)*SIN(P2)
181 R2=(R(J)+R(J+1))*COS(180/N)/2
182 MOVE R2*COS((P1+P2)/2),R2*SIN((P1+P2)/2)
183 PRINT "E";J+M*I
184 NEXT J
185 MOVE R(M+1)*COS(P1),R(M+1)*SIN(P1)
186 DRAW R(M+1)*COS(P2),R(M+1)*SIN(P2)
187 RETURN
188 REMARK Define Sector Windows
189 R1=(R(M+1)+R(1))*COS(360*(I+0.5)/N)/2
190 R2=(R(M+1)+R(1))*SIN(360*(I+0.5)/N)/2
191 F=R(M+1)-R(1)
192 WINDOW R1-F,R1+F,R2-F,R2+F
193 RETURN
194 PRINT "LRun ID = ";T$;"__Calculated Element Geometry"
195 I=1
196 GOSUB 188
197 GOSUB 171
198 FOR J=1 TO M
199 MOVE R(J)*COS(540/N)*COS(180/N),R(J)*SIN(540/N)*COS(180/N)
200 PRINT "B";J;"= ";B(J)
201 R2=(R(J+1)+R(J))/2
```

V(s) — Draw Sector — Define Window — Geometry (B)

```
202 MOVE R2*COS(360/N),R2*SIN(360/N)
203 PRINT "S";J;"= ";S(J)
204 MOVE R2*COS(360/N),R2*SIN(360/N)-0.02*(R(M+1)+R(1))
205 PRINT "A";J;"= ";A(J)
206 NEXT J
207 MOVE P(M+1)*COS(540/N)*COS(180/N),R(M+1)*SIN(540/N)*COS(180/N)
208 PRINT "B";M+1;"= ";B(M+1)
209 PRINT @32,21:110,5
210 INPUT P$
211 GO TO 113
212 FOR I=0 TO N-1
213 PRINT "LRun ID = ";T$;"__Displacement Data"
214 GOSUB 188
215 GOSUB 171
216 FOR J=1 TO M+1
217 MOVE R(J)*COS(P1),R(J)*SIN(P1)
218 PRINT "dY= ";
219 INPUT Y(J,I+1)
220 MOVE R(J)*COS(P1),R(J)*SIN(P1)-0.02*(R(M+1)+R(1))
221 PRINT "dZ= ";
222 INPUT Z(J,I+1)
223 IF I>1 THEN 226
224 Y(J,N+1)=Y(J,1)
225 Z(J,N+1)=Z(J,1)
226 NEXT J
227 NEXT I
228 GO TO 113
229 PRINT "__Input file number = ";
230 INPUT F
231 IF F<=0 THEN 229
232 FIND F+1
233 INPUT @33:Y,Z
234 PRINT "LdY's from File #";F,Y
235 INPUT P$
236 PRINT "LdZ's from File #";F,Z
```

90° (11)

Δ from Key (8)

Δ from Tape (7)

ORIGINAL PAGE IS OF POOR QUALITY

38

Δ To Tape (9)

```
237 GO TO 209
238 PRINT "__Output file number = ";
239 INPUT F
240 IF F<=0 THEN 238
241 FIND F+1
242 PRINT @33:Y;Z
243 GO TO 113
244 P=0
245 F2=0
246 F4=0
247 S2=0
248 PRINT "LRun ID = ";T$;"__Element       U1              U2              ";
249 PRINT " U3               F1              F3_"
250 FOR I=P TO N-1
251 FOR J=1 TO M
252 PRINT "E";J+M*I;"K"
253 P1=360*I/N
254 P2=P1+360/N
255 L1=Y(J+1,I+1)*COS(P1)+Z(J+1,I+1)*SIN(P1)
256 L2=Y(J+1,I+2)*COS(P2)+Z(J+1,I+2)*SIN(P2)
257 L3=Y(J,I+1)*COS(P1)+Z(J,I+1)*SIN(P1)
258 L4=Y(J,I+2)*COS(P2)+Z(J,I+2)*SIN(P2)
259 M1=Y(J+1,I+1)*SIN(P1)-Z(J+1,I+1)*COS(P1)
260 M2=Y(J+1,I+2)*SIN(P2)-Z(J+1,I+2)*COS(P2)
261 M3=Y(J,I+1)*SIN(P1)-Z(J,I+1)*COS(P1)
262 M4=Y(J,I+2)*SIN(P2)-Z(J,I+2)*COS(P2)
263 U1=(L1+L2-L3-L4)/2/S(J)
264 U2=((M1-M2)/B(J+1)+(M3-M4)/B(J))/2
265 U3=((M1+M2-M3-M4)/S(J)+(L1-L2)/B(J+1)+(L3-L4)/B(J))/2
266 C1=(U1+U2)/2
267 C2=SQR((U1-U2)↑2+U3↑2)/2
268 F1=C1+C2*SGN(C1)
269 F2=F2+ABS(F1)*A(J)
270 F3=C1-C2*SGN(C1)
271 F4=F4+(F1↑2+F3↑2)*A(J)
```

```
272 S2=S2+F1*A(J)
273 PRINT USING 274:U1,U2,U3,F1,F3
274 IMAGE 11D.8D,4(4D.8D)
275 IF J+M*I=24 THEN 289
276 NEXT J
277 NEXT I
278 F2=F2/PI/(R(M+1)↑2-R(1)↑2)
279 F4=K*SQR(F4/PI/(R(M+1)↑2-R(1)↑2))
280 S2=S2/PI/(R(M+1)↑2-R(1)↑2)
281 P$="Net tension"
282 IF S2>0 THEN 285
283 P$="Net compression"
284 IMAGE L,"F2, F4 = ",2D.8D,4D.8D,14X,15A/47X,"(",2D.8D,")"
285 PRINT USING 286:K,V
286 IMAGE L,"K, V = ",4D.8D,4D.8D
287 PRINT USING 284:F2,F4,P$,S2
288 GO TO 209
289 P=I+M-1
290 PRINT USING 286:K,V
291 INPUT P$
292 GO TO 248
293 END
```

Program Menu

```
 1. Input Run ID
 2. Input number of sectors                 Default = 16
 3. Input number of annular rings           Default = 2
 4. Input displacement scale                Default = 1
 5. Input Poisson's ratio                   Default = .495
 6. Input annular ring radii                Default = 30.917, 48, 72.74
 7. Input displacements from tape file
 8. Input displacements from keyboard
 9. Output displacements to tape file
10. Output element nomenclature
11. Output calculated element geometry
12. Output propellant dynamic strains
13. Exit program

    Input line number of desired program response : 1

Run ID = FILE
```

ORIGINAL PAGE IS
OF POOR QUALITY

REFERENCES

1. Yorgiadis, A. J.: Dynamic Properties of Inert Propellant for Quarter Scale SRM, Rockwell International Report, March 21, 1977.

2. Hammond, W. E.: Space Shuttle SRM Propellant Dynamic Properties, Thiokol, TWR-11779, March 1978.

3. Francis, E. C.: Research Study of TP-H1148 and Other Similar Solid Propellants, United Technologies, CSD 2608-FR, April 1978.

4. Stoker, J. H.: Space Shuttle SRM Propellant Dynamic Properties, Thiokol, TWR-10543, June 26, 1975.

5. Hufferd, W. L.: Measured Properties of Propellant for SRB One-Eighth Scale Dynamic Shuttle Model, NASA CR-144938, 1975.

6. Hammond, W. E.: Space Shuttle SRM Propellant Dynamic Properties, Thiokol, TWR-12003, October 1978.

7. Parker, G.: SRB Propellant Dynamic Shear Modulus Evaluation, Preliminary, Rockwell International, SOD-79-00-93, January 29, 1979.